
**Pacific Northwest
National Laboratory**

Operated by Battelle for the
U.S. Department of Energy

FY 2006 Miniature Spherical Retroreflectors Final Report

N. C. Anheier
B. E. Bernacki
K. Krishnaswami

December 2006

Prepared for the U.S. Department of Energy
under Contract DE-AC05-76RL01830



DISCLAIMER

This report was prepared as an account of work sponsored by an agency of the United States Government. Neither the United States Government nor any agency thereof, nor Battelle Memorial Institute, nor any of their employees, makes **any warranty, express or implied, or assumes any legal liability or responsibility for the accuracy, completeness, or usefulness of any information, apparatus, product, or process disclosed, or represents that its use would not infringe privately owned rights.** Reference herein to any specific commercial product, process, or service by trade name, trademark, manufacturer, or otherwise does not necessarily constitute or imply its endorsement, recommendation, or favoring by the United States Government or any agency thereof, or Battelle Memorial Institute. The views and opinions of authors expressed herein do not necessarily state or reflect those of the United States Government or any agency thereof.

PACIFIC NORTHWEST NATIONAL LABORATORY

operated by

BATTELLE

for the

UNITED STATES DEPARTMENT OF ENERGY

under Contract DE-AC05-76RL01830

Printed in the United States of America

Available to DOE and DOE contractors from the

Office of Scientific and Technical Information,

P.O. Box 62, Oak Ridge, TN 37831-0062;

ph: (865) 576-8401

fax: (865) 576-5728

email: reports@adonis.osti.gov

**Available to the public from the National Technical Information Service,
U.S. Department of Commerce, 5285 Port Royal Rd., Springfield, VA 22161**

ph: (800) 553-6847

fax: (703) 605-6900

email: orders@ntis.fedworld.gov

online ordering: <http://www.ntis.gov/ordering.htm>



This document was printed on recycled paper.

FY 2006 Miniature Spherical Retroreflectors Final Report

N. C. Anheier
B. E. Bernacki
K. Krishnaswami

December 2006

Prepared for
the U.S. Department of Energy
under Contract DE-AC05-76RL01830

Pacific Northwest National Laboratory
Richland, Washington 99352

Summary

Research done by the Infrared Photonics team at Pacific Northwest National Laboratory (PNNL) is focused on developing miniature spherical retroreflectors using the unique optical and material properties of chalcogenide glass to reduce performance-limiting spherical aberrations. The optimized optical performance will provide efficient signal retroreflection that enables a broad range of remote detection scenarios for mid-wave infrared (MWIR) and long-wave infrared (LWIR) sensing applications. Miniature spherical retroreflectors can be developed to aid in the detection of signatures of nuclear proliferation or other chemical vapor or radiation signatures. Miniature spherical retroreflectors are not only well suited to traditional LIDAR methods for chemical plume detection and identification, but could enable remote detection of difficult semi-volatile chemical materials or low-level radiation sources.

During FY 2006, PNNL's Infrared Photonics research team continued efforts developing miniature spherical retroreflectors based on chalcogenide glass. Optical ray trace modeling and stray light simulation analysis were used to refine the optical performance and to develop optimized optical designs. Baseline optical retroreflection measurements were performed on commercially available high-index ball lenses. The Flow Focusing micro-nozzle retroreflector fabrication approach, explored during FY 2005, was shelved in favor of a more cost-effective compression molding approach. PNNL developed specifications for a custom compression molding press, and then managed the design and fabrication by a commercial company.

Contents

Summary	iii
1.0 Introduction	1.1
2.0 Retroreflector Optical Design Considerations	2.1
2.1 Simple Ball Lens	2.1
2.2 Spherical Gradient Index Ball Lens Retroreflector	2.2
2.3 Step Index Ball Lens Retroreflector	2.3
2.4 Tolerance Analysis	2.5
3.0 Retroreflector Performance Characterization.....	3.1
3.1 Experimental Apparatus	3.1
3.2 Ball Lens Retroreflection Characterization	3.2
4.0 Retroreflector Fabrication	4.1
4.1 Retroreflector Glass Selection.....	4.1
4.2 Compression Molding Press.....	4.3
4.2.1 Press Specifications.....	4.4
4.2.2 Press Design and Construction Progress	4.4
5.0 Summary	5.1
6.0 References	6.1

Figures

2.1	Spherical Retroreflector Structure Proposed for Laser Tracking Described by Yingbing et al. (2003).....	2.1
2.2	Index Profile Obtained from an Optimized Design for a Spherical Gradient Ball Lens Having a Surface Index of $n = 2.77$	2.2
2.3	Step Index Mid-IR Retroreflector Constructed with a 5-mm Diameter ZnS Core and a 1.42 mm Thick IG3 Cladding	2.3
2.4	Return Fraction Versus Cladding Reflectance Showing that the Maximum Return from the Ball Retroreflector Occurs When r is Equal to 0.33	2.4
2.5	Schematic of the Composite Step Index Retroreflector Described in Oakley.....	2.4
2.6	Strehl Ratio Versus Cladding Thickness Variation from the Design Value.....	2.5
2.7	Strehl Ratio Versus Cladding Thickness for Central Cores Having a Variation in Thickness of $\pm 10 \mu\text{m}$	2.6
3.1	Apparatus for Measuring the Miniature Spherical Retroreflector Performance.....	3.1
3.2	Spatial Profile of the Retroreflected Data Acquired from a 5-mm S-LAH79 Ball Lens Illuminated with a HeNe Laser.....	3.2
3.3	Simulation of the Retroreflection from a S-LAH79 Ball Lens Fitted to the Data Acquired With the Apparatus Described Above.....	3.3
3.4	Images of the Retroreflected Beam Features from BK7, Sapphire, LASFN9, and S-LAH79 Ball Lenses	3.4
4.1	Logarithmic Viscosity as a Function of Linear Temperature for Potential Chalcogenide Cladding Glasses	4.2
4.2	Front View of the Compression Molding Press that will be Used to Fabricate Clad-Ball Retroreflector Devices	4.5
4.3	Rear View of the Compression Molding Press	4.5

Tables

4.1	Potential Infrared Glasses for the Retroreflector Fabrication.....	4.2
-----	--	-----

1.0 Introduction

A miniature spherical retroreflector has a number of unique properties that make it attractive for many remote sensing applications. A spherical retroreflector can be deployed without concern of precise placement because the spherical geometry provides an omni-directional return. This omni-directional property is due to the sphere's lack of optical axis and it facilitates remote interrogation from wide-angle land or aerial advantages. Incident laser illumination is collected and tightly focused by the sphere at the sphere glass-air interface, where laser-induced fluorescence methods can be employed to detect the presence of either chemical or radiation sources, at large standoff distances. Two detection strategies include a sphere coated with either a radiation- or chemical-sensitive fluorescence material (chemical or radiation detection) or with an optically stimulated luminescent material (radiation detection). Since the fluorescence emanates from a point source, the sphere collects and collimates this emission and then directs it back to the laser transceiver. The target sphere diameter is in the range of 5 to 10 mm. They can be easily deployed in large numbers, yet remain indistinguishable from the background environment.

Two main challenges have limited widespread adoption of the miniature spherical retroreflector approach. These challenges are the subject of this PNNL investigation and include: 1) resolving the performance-limiting spherical aberration and 2) developing a practical fabrication approach. During FY 2005, PNNL performed optical simulations to assess potential design improvements over the traditional homogeneous ball lens retroreflector (Anheier et al. 2005). Improvements in retroreflector performance were developed using infrared transparent chalcogenide glass and a step index, clad ball lens design. Three potential methods were suggested for manufacturing these elements, two utilizing variations on compression molding and the third based on a flow-focusing micro-nozzle. The micro-nozzle technique was shelved in favor of the more cost-effective compression molding approach.

In this report we provide a summary of the FY 2006 research progress for the Miniature Spherical Retroreflector project (PL211A). In Section 2, we discuss the step index ball lens retroreflector design using a ZnS core and an IG3 glass cladding, and then provide insight from the fabrication tolerance analysis. In Section 3 we discuss the baseline optical retroreflection measurements performed on commercially available homogeneous ball lenses, and in Section 4 we discuss the infrared glass selection criteria for the step index design and the compression molding fabrication approach.

2.0 Retroreflector Optical Design Considerations

2.1 Simple Ball Lens

The simple ball lens was described in PNNL's previous report (Anheier et al. 2005) to motivate the reason for embarking on the path of research described within this report. It was shown, as have other authors (Takatsuji et al. 1999), that for a homogeneous lens the optimum design conditions for maximum retroreflection of the beam occurs when $n = 2$ at the wavelength of use for the sphere. However, this is only a paraxial approximation and practical beams having a finite extent produce significant spherical aberration as the diameter of the incident beam approaches the size of the physical aperture of the retroreflector, and this spoils the retroreflector return efficiency. Furthermore, a practical optical material exists only in the regime of visible optics, as one can use S-LAH79 glass with $n = 2.0$ at 600 nm to produce optimum miniature spherical retroreflectors. No such glass exists in the mid-IR ($3 \mu\text{m}$ to $12 \mu\text{m}$), where the lowest-index glass type available is ZnS, which has an index of 2.20 at $10 \mu\text{m}$. Therefore, a clad design that consists of a spherical core embedded in a *hemispherical* shell to take advantage of the step index at the rear (reflective) surface, with half of the core (the incident surface) immersed in air, as shown in Figure 2.1, has been proposed to reduce the aberrations (angular divergence) of the return beam, much like the principles employed in optical doublet design (Yingbing et al. 2003). However, PNNL's program requires an isotropic structure to provide an omni-directional retroreflection, unlike the spherical retroreflectors described in Yingbing et al. (2003). A marked improvement in a potential isotropic miniature spherical retroreflector design is based on a gradient index approach, and is discussed next.

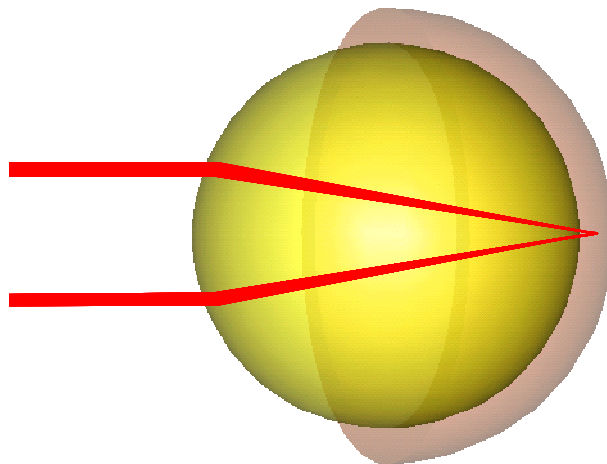


Figure 2.1. Spherical Retroreflector Structure Proposed for Laser Tracking Described by Yingbing et al. (2003). Since the structure can be oriented in a mounting structure, the anisotropic ball structure can be used. PNNL's program requires an isotropic structure that provides an omni-directional retroreflection.

2.2 Spherical Gradient Index Ball Lens Retroreflector

Some IR glasses, notably the chalcogenide varieties, can have their index modified by light (photomodification) by illumination having a wavelength near the band gap of the material, where it is strongly absorbed. It is, therefore, reasonable to seek a gradient index solution having spherical symmetry, perhaps using chalcogenide glass that has been photomodified to produce a gradient index distribution. The archetypal symmetrical gradient index structure is the Luneburg lens, which has an index profile such that a plane wave (collimated beam) incident on its front surface will be perfectly imaged at the rear of the ball and, hence, reflected without aberration in the reverse direction along the incident path to the illumination source. The index profile for a Luneburg lens is given by (Born and Wolf 1980):

$$n(r) = \sqrt{2 - \left(\frac{r}{a}\right)^2}.$$

In this expression r is the distance from the center of the ball and a is the radius of the ball. Immediately one sees at the surface of the ball immersed in air, the index at the outer surface of the sphere must be equal to one when r is equal to a ! Thus, this structure is not physically realizable. However, one can make a reasonably good approximation to a Luneburg lens in theory by designing a spherical gradient index lens with index values $\neq 1$ at the surface of the sphere. If we chose a starting index equal to say, As_2Se_3 at $10 \mu\text{m}$, $n = 2.77$, we can obtain a design that results in an index profile like that shown in Figure 2.2. At present, there is no known method for achieving the large (0.54) change in index in a

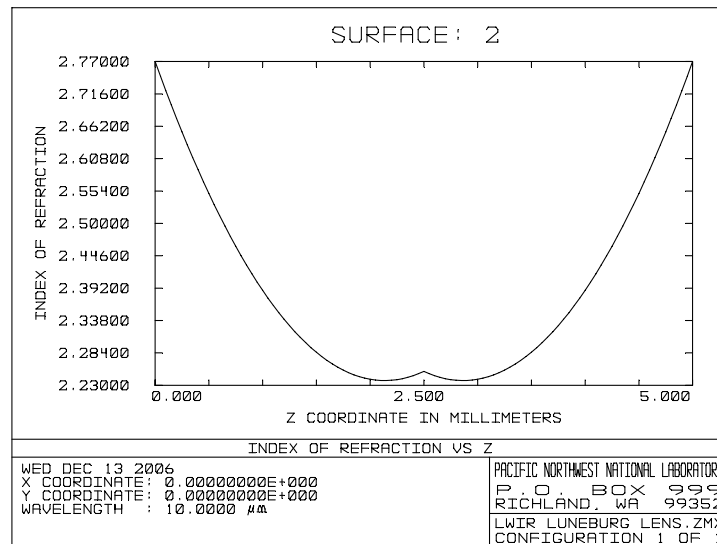


Figure 2.2. Index Profile Obtained from an Optimized Design for a Spherical Gradient Ball Lens Having a Surface Index of $n = 2.77$. Note that design change in index is 0.54, which is not attainable by any presently known gradient index manufacturing method.

gradient index material needed to produce this profile. The magnitude of index change possible due to photomodification in currently known chalcogenide glasses would most likely not exceed 0.05 at $\lambda = 10 \mu\text{m}$. Therefore, a gradient index approach will not yield acceptable results for a mid-IR miniature spherical retroreflector.

2.3 Step Index Ball Lens Retroreflector

Since the spherical gradient index retroreflector design analysis resulted in greatly improved optical performance when compared with a homogeneous IR glass design (even if it is not attainable in practice), we proposed earlier to approximate the continuous change in index needed with a step index profile. The design that resulted is shown in Figure 2.3. The core is constructed of ZnS that has an index of 2.20 at a wavelength of $10 \mu\text{m}$, and an outer cladding 1.36-mm thick constructed of $\text{Ge}_{30}\text{As}_{13}\text{Se}_{32}\text{Te}_{25}$ (known as IG3 glass from Vitron Spezialwerkstoffe GmbH). A compression molding approach to cladding a higher- T_g core with a low- T_g moldable glass was proposed as one of the construction methods in the previous report and has been selected as the primary method of producing a mid-IR miniature spherical retroreflector. One interesting observation contained in a not-yet-published paper^(a) or a concentric double clad retroreflector similar to our proposed design is that an optimum multi-layer coating exists that maximizes the return from the rear surface of an isotropic retroreflector. At normal incidence, the magnitude of the reflected signal for a unity amplitude input beam can be expressed as:

$$R_{total} = r(1 - r)^2$$

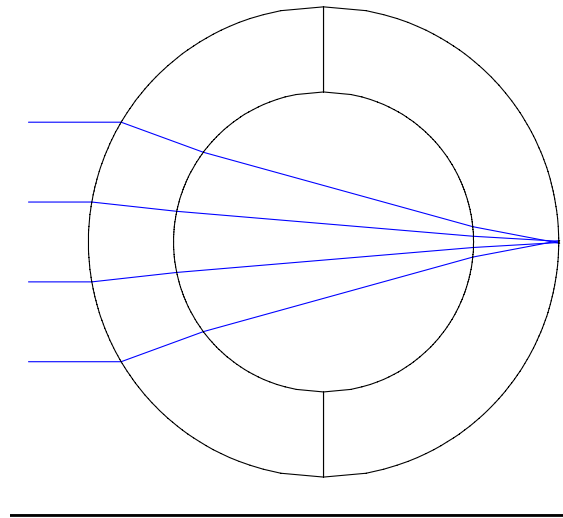


Figure 2.3. Step Index Mid-IR Retroreflector Constructed with a 5-mm Diameter ZnS Core and a 1.42-mm Thick IG3 Cladding

(a) Oakley JP. "Whole-angle spherical retro-reflector using concentric layers of homogenous optical media," *Appl. Opt.*, to be published.

By taking the first derivative and setting it equal to zero, it can be shown that the maximum return occurs when the reflectivity r is equal to 0.33. This simple expression does not take into effect the small losses at the glass-glass interfaces. A plot of R_{total} versus reflectivity is shown in Figure 2.4. When r is equal to 0.33, the maximum return efficiency from the retroreflector is 14.8%.

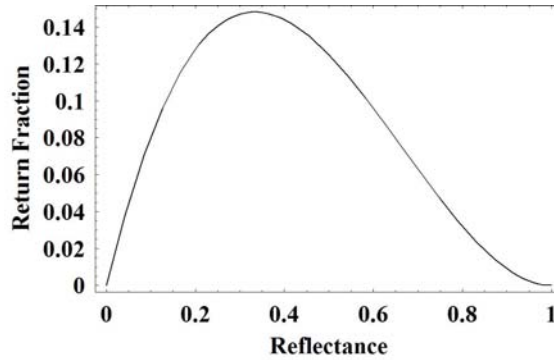


Figure 2.4. Return Fraction Versus Cladding Reflectance Showing that the Maximum Return from the Ball Retroreflector Occurs When r is Equal to 0.33

Since the index of IG3 is 2.7870 at 10 μm , the reflectance at normal incidence in air is 22.3%, which results in a return fraction of 13.5%, only 1.3% less than the theoretical maximum. Therefore, special multi-layer coatings to achieve a higher reflectance of 33.3% are not warranted. Besides the Oakley paper, others (Burmistrov et al. 2002) have constructed large isotropic step index spherical retroreflectors that were fabricated using traditional grinding and polishing and assembled manually. The Oakley retroreflector is shown in Figure 2.5. It is unclear if an additional layer would be worth the added complexity for the PNNL development effort, but this will be investigated in the coming year. The lack of variety of optical materials in the mid-IR does not bode well for a three-layer solution.

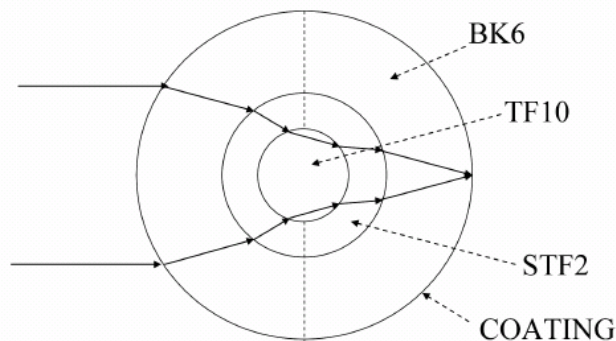


Figure 2.5. Schematic of the Composite Step Index Retroreflector Described in Oakley^(a)

(a) Oakley JP. "Whole-angle spherical retro-reflector using concentric layers of homogenous optical media," *Appl. Opt.*, to be published.

2.4 Tolerance Analysis

Compression-molded optical elements require that the glass preform used for the part be held to relatively tight tolerances as the *volume* of the preform must be strictly controlled to result in an optical element having the appropriate design dimensions. The core of the proposed design is essentially a ZnS ball lens that is obtained commercially^(a) and has a diameter tolerance of $\pm 10 \mu\text{m}$. The cladding preform, a disk of IG3 glass, can be reasonably manufactured to maintain its thickness to $\pm 100 \mu\text{m}$ if we consider commercial-grade specifications, but certainly tighter tolerances are possible for slightly more cost. Typically, window thickness is not critical for functionality, and optical windows are optimized for minimum surface flatness and roughness with more relaxed thickness tolerances to minimize manufacturing cost and throughput. Modeling was performed to see how the Strehl Ratio varies with cladding thickness. The Strehl Ratio is a single figure of merit defined as the ratio of the peak of the diffraction pattern of an aberrated image formed by an optical system to that of an unaberrated image formed by the same system. Mathematically, it is approximately equal to (Smith 2005):

$$SR = 1 - (2\pi\sigma)^2.$$

The quantity σ is the RMS wavefront error (WFE). The diffraction limit using Strehl criteria is defined as 0.8, which equates to an RMS WFE of 0.07λ ($\lambda/14$). The Strehl Ratio of the focused spot at the rear surface of the spherical retroreflector versus the variation in cladding thickness from the nominal value is depicted in Figure 2.6 for $\pm 130 \mu\text{m}$ variation from the ideal cladding thickness. Note that the performance ceases to be diffraction-limited when the variation in cladding thickness exceeds $\pm 50 \mu\text{m}$.

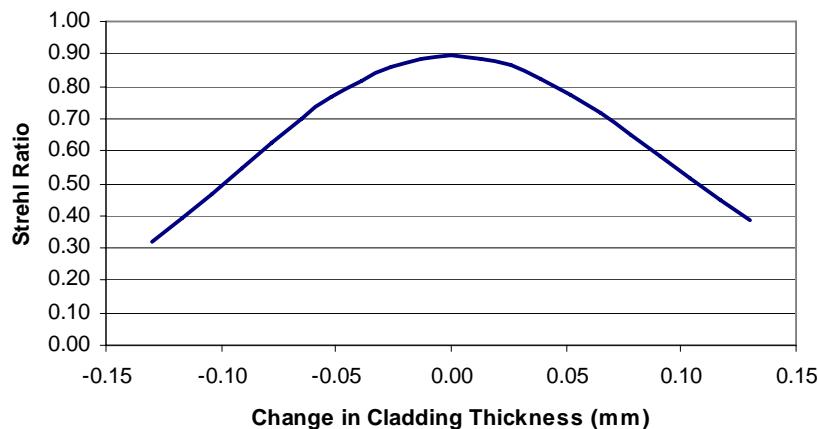


Figure 2.6. Strehl Ratio Versus Cladding Thickness Variation from the Design Value. Note that the device can remain diffraction-limited if the cladding thickness variation is within $\pm 50 \mu\text{m}$ ($SR < 0.8$).

(a) ISP Optics, Irvington, New York, <http://www.ispoptics.com>.

In the case of a variation in ball thickness, the resulting design is barely changed, and has the effect of shifting the performance curves shown in Figure 2.7 laterally about the curve shown for the design having the ideal nominal central ball thickness. It is evident, therefore, that the main influence on performance will be thickness variation in the cladding thickness. Most likely, the best route to manufacturability is to ensure there is *enough* thickness so that it can be polished back to the design value. There will be a molding artifact where the two retroreflector cladding halves join that will require some post polishing to reduce scatter. Therefore, both molding artifact removal and dimensional correction can be performed at the same time with the added benefit of reducing the optical tolerances and thus manufacturing cost.

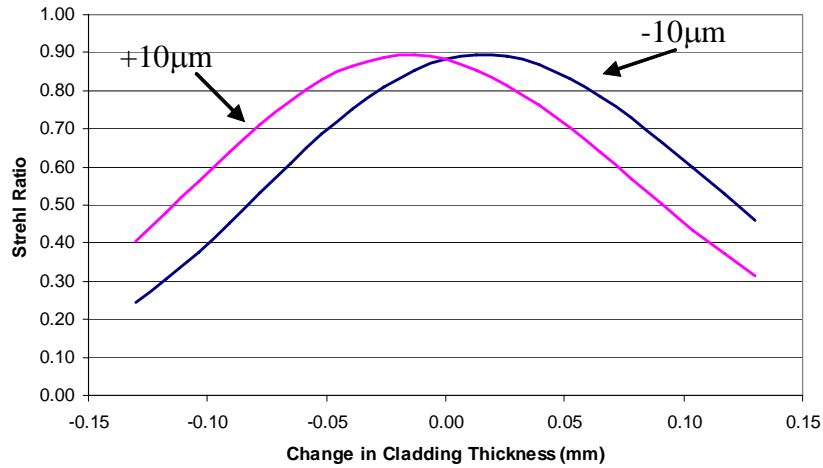


Figure 2.7. Strehl Ratio Versus Cladding Thickness for Central Cores Having a Variation in Thickness of $\pm 10 \mu\text{m}$

3.0 Retroreflector Performance Characterization

Innovative design and fabrication approaches are being developed to reduce the performance-limiting spherical aberrations present in homogeneous ball lens designs. In conjunction with this design and fabrication effort, an apparatus to characterize miniature spherical retroreflector performance has been developed. Commercial homogeneous ball lenses were measured to assess the utility of this apparatus for retroreflector optical efficiency characterization.

3.1 Experimental Apparatus

The apparatus shown in Figure 3.1 comprises of a spatially filtered, expanded, and collimated HeNe laser (632.8 nm) beam to provide uniform illumination over an area of ~25 mm in diameter. A large area ($76.2 \times 76.2 \text{ mm}^2$) cube beam-splitter is incorporated in the apparatus to collect both the retroreflected beam and scatter from its surfaces, then direct it towards a photodetector equipped with a 200- μm diameter aperture. The beam-splitter was placed at a small angle to separate the retroreflected beam from the internal reflections produced within the beam-splitter. The retroreflected beam features were acquired by scanning the detector assembly, in steps sizes ranging from 2 to 10 μm , using a computer-controlled linear stage.

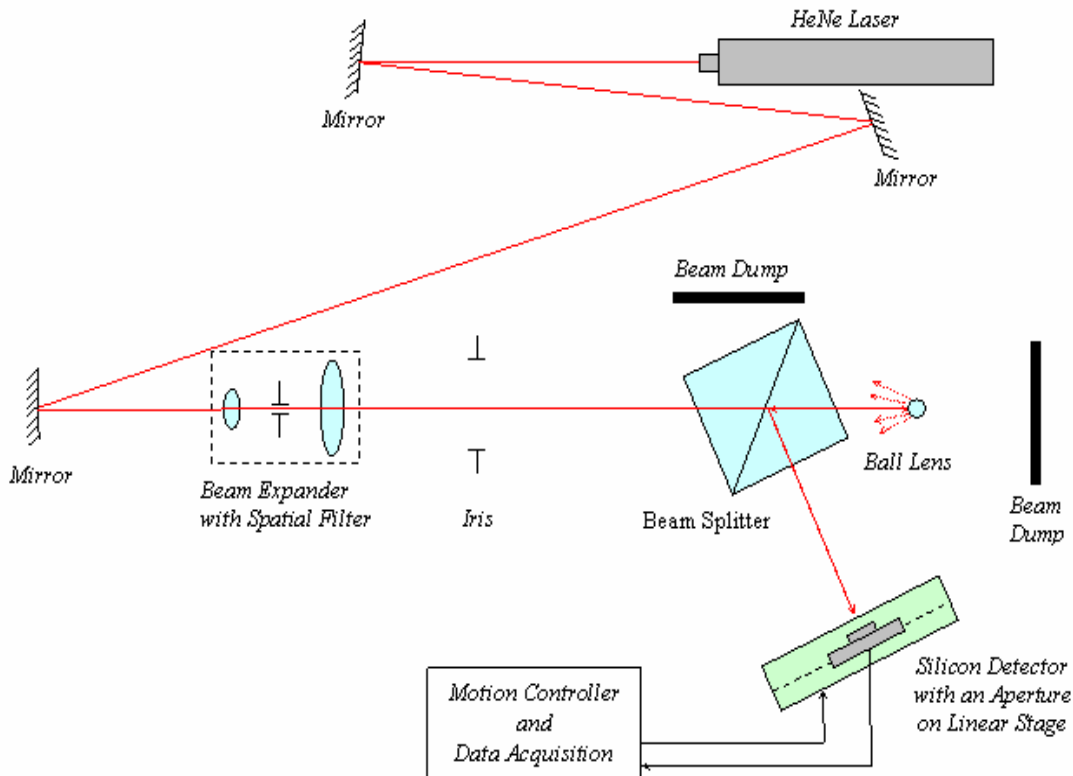


Figure 3.1. Apparatus for Measuring the Miniature Spherical Retroreflector Performance

3.2 Ball Lens Retroreflection Characterization

Measurements of retroreflected signals from a S-LAH79 ball lens were first acquired. This ball lens, procured from Edmund Optics, had a refractive index of 2.003 and a diameter of 5 mm. The distance from the ball lens to the detector was approximately ~ 190 mm. The spatial profile of the retroreflected beam, measured with a step size of $2\ \mu\text{m}$, is shown in Figure 3.2. The spatial profile shows a strong retroreflected signal along with additional structure due to diffraction from the edges of the ball lens and scatter from its surface.

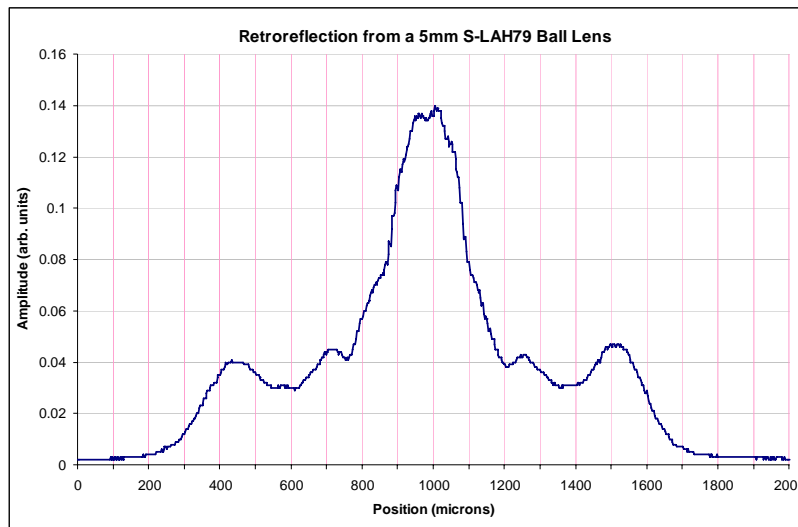


Figure 3.2. Spatial Profile of the Retroreflected Data Acquired from a 5-mm S-LAH79 Ball Lens Illuminated with a HeNe Laser

A retroreflection simulation for the S-LAH79 ball lens was performed using TraceProTM illumination analysis software. The normalized results of the simulated and acquired data are shown in Figure 3.3. It can be seen that there is good correlation between the acquired and simulated data. Since the simulations do not account for diffraction effects, it does not provide some of the finer structure that was observed in measurement.

Retroreflected beam features from ball lenses made from BK7, sapphire, and LASFN9 with refractive indices of 1.517, 1.770, and 1.850 were also measured. However, due to their highly divergent spatial profile, acquiring accurate line scans of the retroreflected signals was not possible. Figure 3.4 shows images of the retroreflected beam features for the four ball lenses. It can be seen that as the index of refraction increases from 1.5 to 2.0, the retroreflection halo diameter is reduced, indicating reduced beam divergence and improved retroreflector efficiency. It was found that for inefficient optical retroreflectors, imaging the return halo provided a coarse estimate of performance, while the scanning apparatus was most suited for optically efficient retroreflectors.

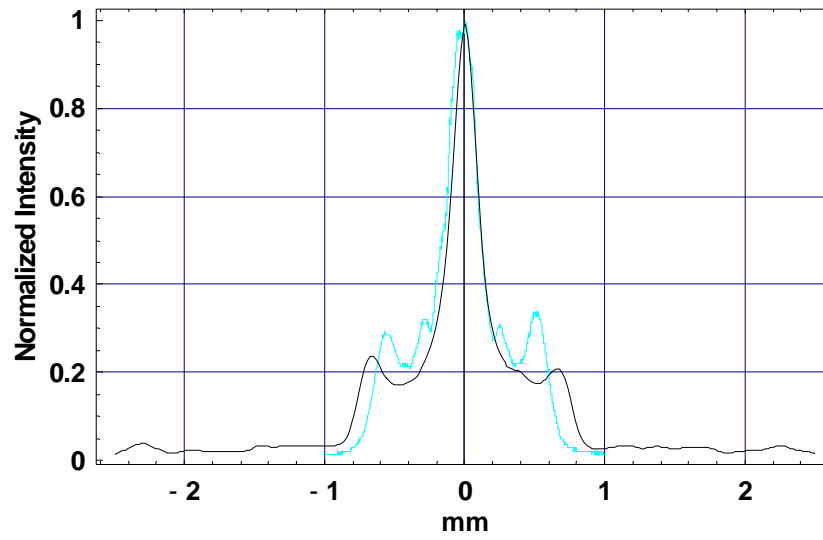


Figure 3.3. Simulation (black line) of the Retroreflection from a S-LAH79 Ball Lens Fitted to the Data (turquoise line) Acquired With the Apparatus Described Above

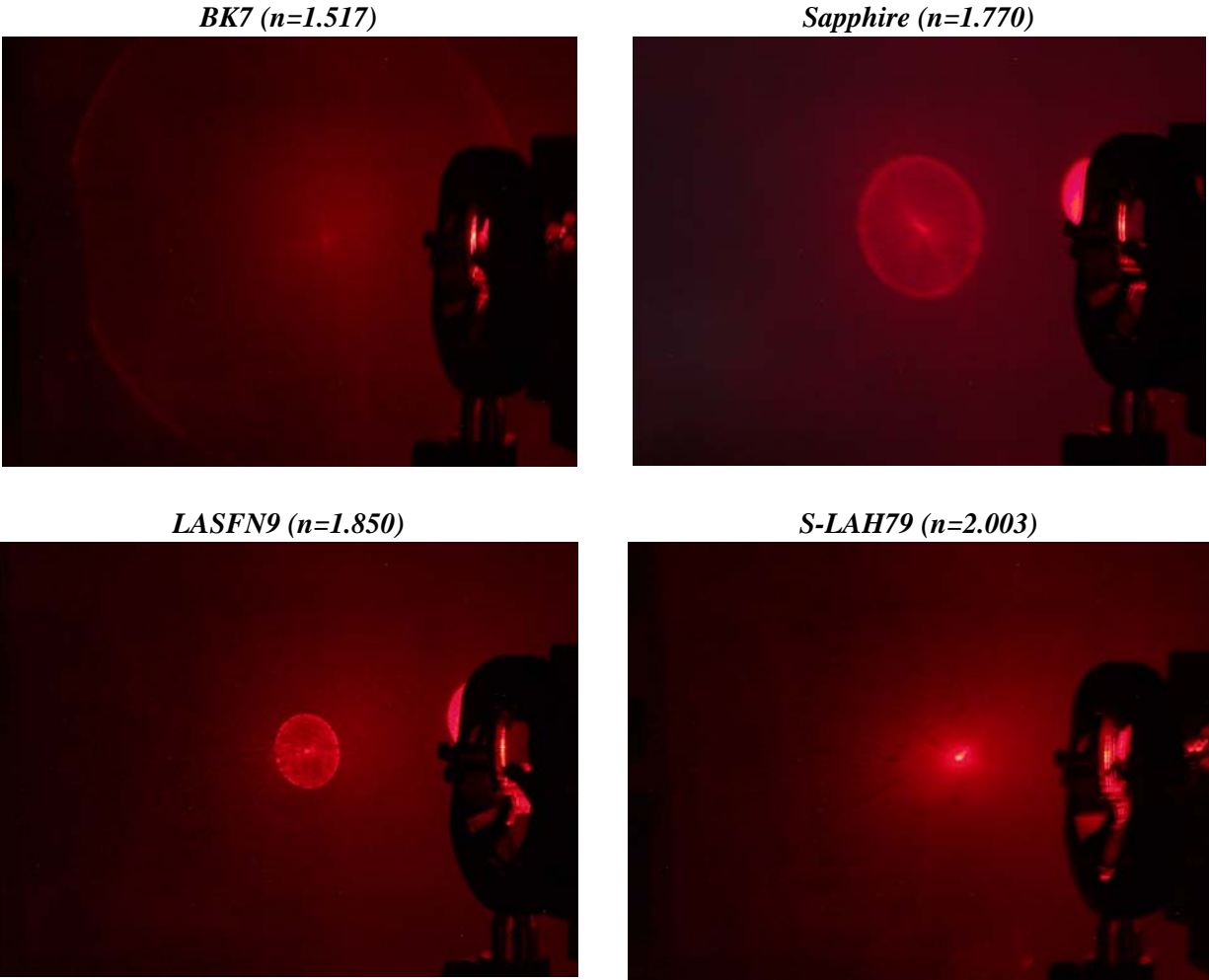


Figure 3.4. Images of the Retroreflected Beam Features from BK7, Sapphire, LASFN9, and S-LAH79 Ball Lenses. It can be seen that as the index of refraction increases from 1.5 to 2.0, the retroreflection halo diameter is reduced, indicating reduced beam divergence and improved retroreflector efficiency.

4.0 Retroreflector Fabrication

The flow-focusing micro-nozzle retroreflector fabrication approach, explored during FY 2005, was shelved in favor of a more cost-effective, lower risk compression molding approach. PNNL developed specifications for a custom compression molding press, and then managed the design and fabrication by a commercial company. Infrared transparent optical glasses were selected for the retroreflector core and clad based on their compatibility with the compression molding process and the required optical performance of the miniature spherical retroreflector.

4.1 Retroreflector Glass Selection

The viscosity of chalcogenide glasses spans about 15 powers of 10 between melting temperature and room temperature, as shown in Figure 4.1. At viscosities between 10^4 and 10^{13} dPa·s the glass transitions from a flowing state to a plastic state. Viscosities above 10^9 dPa·s become less temperature dependent and increasingly time dependent. Glass can be described as solidified or “frozen” at viscosities greater than 10^{13} dPa·s. The glass transition point, T_g , is defined at 10^{13} dPa·s. At this point the glass transitions from a glass to a plastic state and is manifested by a slope change in the coefficient of thermal expansion. The upper annealing point is around 10°C above T_g . The fluidity at this viscosity is just enough to relieve internal stresses within the glass by uniform heating at this temperature for about 30 minutes. Temperatures above the upper annealing point may result in deformation in precision optical surfaces. At the softening point, $T_{s,p} = 10^{7.6}$ dPa·s, glass structures deform under their own weight due to the fluidity of the glass.

Understanding thermo-viscosity behavior of chalcogenide glass is extremely important when developing compression molding processes. For example, slumping the cladding half shell must be done at a high enough temperature for the glass to deform under its own weight, yet at low enough temperatures to prevent dissociation of the compositional elements. The compression molding process can be performed at lower temperatures, where the glass remains in a plastic state, yet can be shaped under the high pressure provided by the molding press. The molding processing is completed by uniformly heating the finished retroreflector at the upper annealing point for 30 minutes to minimize residual internal stress.

Table 4.1 shows the potential infrared glass useful for the retroreflection fabrication. Chalcogenide glasses are the only known IR materials compatible with compression molding due to their low T_g properties. The step index ball lens design described in Section 2 is constructed using a low index (near $n = 2.0$) ball lens clad by a higher index glass shell to reduce the spherical aberrations. ZnS glass is quite possibly the only practical choice for the retroreflector core selection. It has the required infrared transmission from 0.37 to 14 microns, a high $T_{s,p}$, and a relatively low optical index ($n = 2.201$ at $10\ \mu\text{m}$ wavelength). While commercial ZnS ball lenses are not available off-the-shelf, they are available on a custom fabrication basis from a variety of vendors. Also shown in Table 4.1 are two chalcogenide glasses that can be used for the cladding layer, IG3 and $\text{As}_{40}\text{Se}_{60}$. Both glasses are available from commercial sources in both bulk and window format. These glasses have large enough optical indices to significantly reduce the performance-limiting spherical aberrations. The main distinction between the two glass cladding options is the coefficient of thermal expansion (CTE).

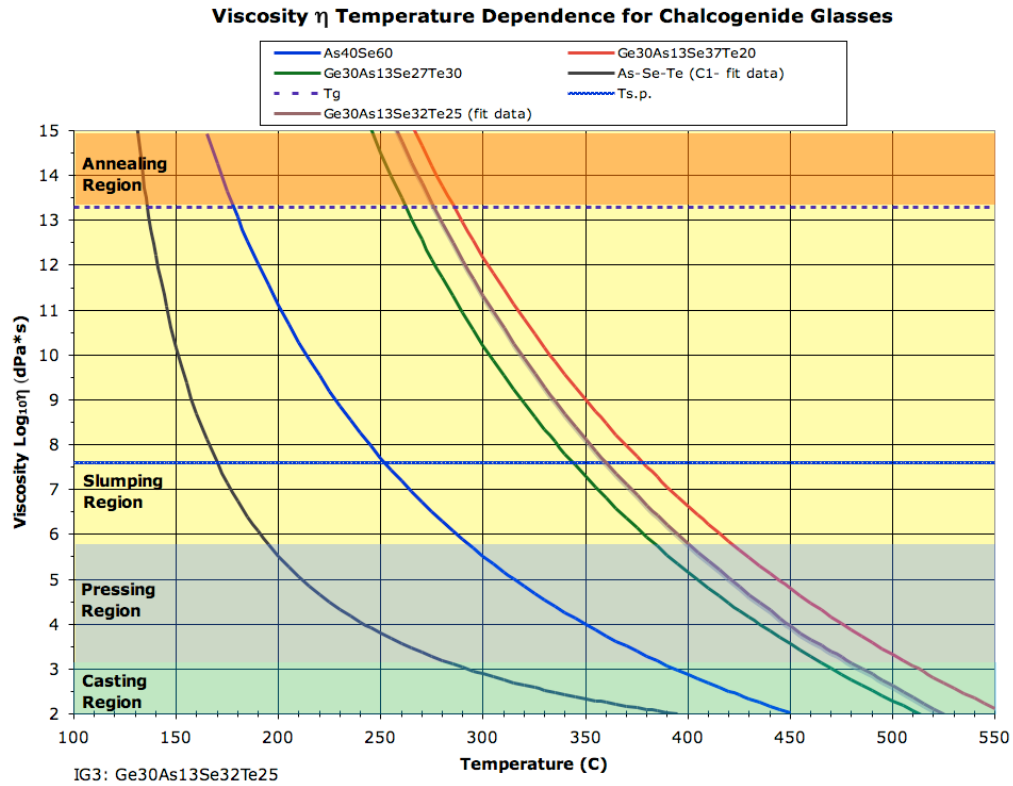


Figure 4.1. Logarithmic Viscosity as a Function of Linear Temperature for Potential Chalcogenide Cladding Glasses. This data was generated using the semi-empirical Vogel-Tammann-Fulcher equation.

Table 4.1. Potential Infrared Glasses for the Retroreflector Fabrication. The infrared glasses noted in red are the optimal choices for the step index, ball lens retroreflector design.

Glass Composition	Core or Clad?	Transmission Window (microns)	Index at 10 μm	Thermal Expansion $\times 10^{-6}/\text{C}$	Softening Point C	Commercial Ball Lenses Available	Commercial Vendor
Ge33As12Se55 (AMTIR1)	Core	0.9-14	2.497	12.1	445	No	Vitron/ Amorphous Materials
GaLaS (GLS)	Core	0.5-10	<2.37?	10	660	Yes	Southampton?
ZnS	Core	0.4-15	2.201	6.5	High	Custom	Various
ZnSe	Core	0.5-18	2.403	7.57	High	Yes	Various
Ge30As13Se32Te25 (IG3)	Clad	1.1-14	2.787	13.4	360	n/a	Vitron
As40Se60	Clad	0.9-15	2.778	20.7	236	n/a	Vitron/ Amorphous Materials

As mentioned above, to assure that the core is not distorted by the over molding process, the core must have a transition temperature T_g much greater than that of the cladding. Fortunately, the crystalline

ZnS core has a very high T_g of approximately 1850°C. With a high T_g comes a low coefficient of expansion (CTE), and conversely, a low T_g results in a high CTE value. For ZnS, the CTE is 6.8 ppm/°C, and for IG3 the CTE is 13.4 ppm/°C, or roughly 2X that of the core. Fortunately these properties are favorable for the molding process, since the clad will shrink around the core when the part cools, placing the core in compression. If the CTE values were switched, the cladding glass would have significant tensile stress and the cladding would likely delaminate from the core.

However, it is worth examining its environmental effects of operating at elevated temperatures to determine if we can, under reasonable operational circumstances, cause the cladding to delaminate from the core. First, we examine the change in dimension of the core at 80°C.

$$\Delta_{core} = 5mm(1 + 6.8 \times 10^{-6} \frac{mm}{mm \text{ } ^\circ C} 80^\circ C) = 5.00272mm$$

The core diameter only grows by 2.72 μm at 80°C. Now for the cladding, we have:

$$\Delta_{clad} = 1.362708mm(1 + 13.4 \times 10^{-6} \frac{mm}{mm \text{ } ^\circ C} 80^\circ C) = 1.36417mm$$

which corresponds to an increase in clad thickness of 1.46 μm . Viewed another way, the outer shell experiences a change in diameter of 2.92 μm that almost matches the core growth. Therefore, we have a relatively balanced condition for the IG3 glass clad at elevated temperatures that should result in minimal stress and a low probability of delamination. This analysis indicates that a ball lens core made of ZnS and a cladding layer made of IG3 chalcogenide glass is the optimal choice for the miniature spherical retroreflector design.

4.2 Compression Molding Press

Fabrication of a clad retroreflector for miniature retroreflectors has been described using compression molding of low T_g IR glass. In the case of the miniature IR retroreflector, the fabrication approach presented involves molding a chalcogenide cladding about a central crystalline ball lens core. In the design chapter, it was shown that only a Luneburg lens provides a perfect retroreflected beam across its entire aperture. Unfortunately, the boundary conditions of the spherical gradient Luneburg lens are unattainable (the index must have the same value of the immersion medium, which means $n = 1$ in air), and the magnitude of the index change required is also not attainable by any presently practiced gradient optics manufacturing method. Therefore, the step index or clad ball approach was developed to coarsely approximate the gradient index necessary to optimize the return from the rear surface of the retroreflector when the outer surface consists of the commercial IG3 chalcogenide glass available from Vitron.

It was shown that an ideal paraxial ball retroreflector made of homogeneous glass must have an index of $n = 2$ for perfect retroreflection on-axis, but spherical aberration increases as the size of the entrance pupil increases, with the magnitude of spherical aberration reaching its maximum at the physical diameter of the ball lens. However, the material order for a symmetric clad retroreflector in terms of index is H-L-H, with the low index (L) central core consisting of a ZnS ball and the high index (H) shell consisting of chalcogenide glass. ZnS is a crystalline material grown by CVD with an index of 2.20 at 10.0 μm and a

melting point of about 1850°C which is well below the 275°C T_g for IG3. Due to the high melting point of ZnS, the clad molding operation will not cause any deformation of the ZnS core.

4.2.1 Press Specifications

A glass molding press needed to produce the clad ball retroreflector devices is under construction at Dyna Technologies, Inc. in Sanford, Florida. The details of the glass shell molding process can be found in the FY 2005 report (Anheier et al.2005). The molding press will have the following capabilities:

- Capacity. The press can mold objects up to 25 mm in diameter.
- Temperatures Control. The press can provide heating up to 500°C \pm 5°C controlled by active PID control, has a method for active temperature control by using cooling by fluids, and the temperature setting and profile is computer controlled.
- Molding Force and Precision. The press has an electric screw actuator with 400 pounds of force with integral encoder to enable closed loop positioning with \pm 10 mm of accuracy. Force feedback will also be provided by a load cell. The support structure will minimize deflection due to molding forces and dimensional changes due to temperature changes during the molding cycle.
- Mold Technology. The press will be able to use both metallic and ceramic molds with an insert approach.
- Molding Atmosphere. The region containing the mold halves will be able to be purged to ensure the molding atmosphere is not reactive. Most likely, the molding region will be evacuated and backfilled with nitrogen to minimize glass oxidation under elevated temperatures and pressures.
- Machine Control. The press will be controlled by PLC but can also be controlled by personal computer under LabVIEW™ control if desired.

4.2.2 Press Design and Construction Progress

A front view of the press is shown in the Figure 4.2. The support electronics and electrical controls are housed in the cabinet to the left, while the ram and mold assembly is visible in the right section. A rear view of the press is shown in Figure 4.3. As of the end of calendar year 2006, the press was approximately 60% complete at our external vendor's facility and a February 2007 delivery is anticipated.

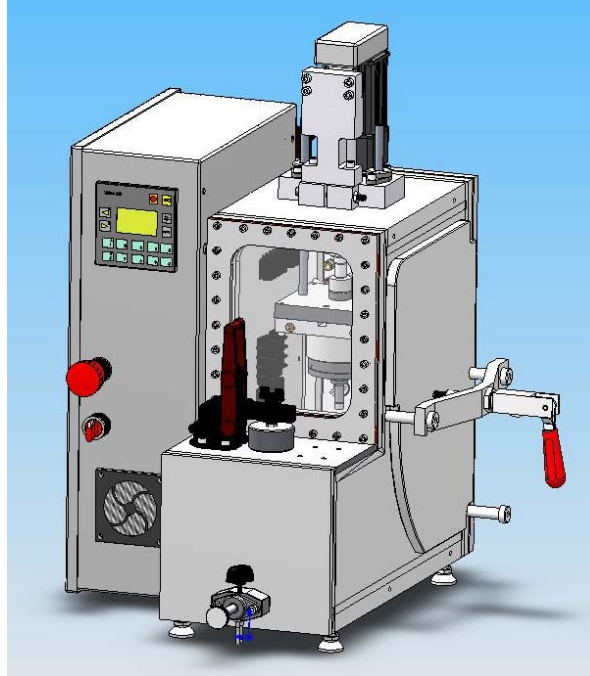


Figure 4.2. Front View of the Compression Molding Press that will be Used to Fabricate Clad-Ball Retroreflector Devices

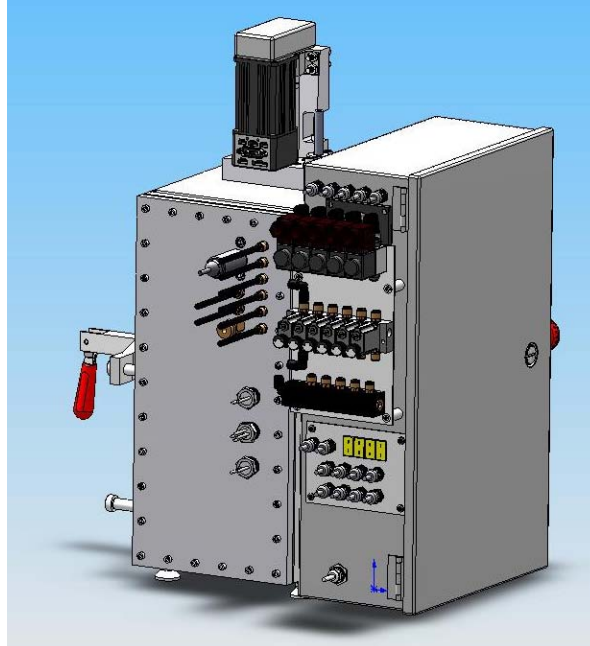


Figure 4.3. Rear View of the Compression Molding Press. The electrical cabinet on the right is equipped with terminals for power and control signals. The molding cabinet on the left has feedthroughs for power and control as well as vacuum and fluid (N₂) feedthroughs for molding atmosphere and cooling.

5.0 Summary

During FY 2006, PNNL's Infrared Photonics research team continued efforts to develop miniature spherical retroreflectors based on chalcogenide glass. Optical ray trace modeling and stray light simulation analysis were used to refine the optical performance and to develop optimized optical designs. Homogeneous glass ball lenses, while ubiquitous and inexpensive, cannot return the input beam with high enough efficiency over a large aperture to make them worthwhile candidates for high-performance remote sensing applications. Step index ball lens retroreflector designs, using a ZnS core and an IG3 glass cladding, show both promising infrared performance and practical fabrication potential. Fabrication tolerance analysis revealed that molding the retroreflector with a slightly larger diameter, then performing a final artifact removal and diameter correction by post polishing, might alleviate strict cladding thickness requirements.

Baseline optical retroreflection measurements were performed on commercially available homogeneous ball lenses. The flow-focusing micro-nozzle retroreflector fabrication approach, explored during FY 2005, was shelved in favor of a more cost-effective compression molding approach. PNNL developed specifications for a custom compression molding press, and then managed the design and fabrication by a commercial company. During FY 2007, PNNL plans to investigate fabrication methods, for the step index retroreflector approach, using this custom compression molding press.

6.0 References

Anheier NC, BE Bernacki, BR Johnson, BJ Riley and WA Sliger. 2005. *FY 2005 Miniature Spherical Retroreflectors Final Report*. PNNL-15577, Pacific Northwest National Laboratory, Richland, Washington.

Born M and E Wolf. 1980. *Principles of Optics, 6th Ed.* Pergamon Press, New York, p. 147.

Burmistrov V, N Parkhomenko, Y Roy, V Shargorodsky, JD Vasiliev, S Habib, V Glotov and N Sokolov. 2002. "Spherical retroreflectors with an extremely small target error: International experiment in space," *Proceedings of the 13th International Workshop on Laser Ranging*, Washington, D.C.

Smith WJ. 2005. *Modern Lens Design: 2nd Ed.* McGraw-Hill, New York, p. 72.

Takatsuji T, M Goto, S Osawa, R Yin and T Kurosawa. 1999. "Whole-viewing-angle cat's eye retroreflector as a target of laser trackers," *Meas. Sci. Technol.*, **10**, N87-N90.

Yingbing L, Z Guoxiong and L Zhen. 2003. "An improved cat's eye retroreflector used in a laser tracking interferometer system," *Meas. Sci. Technol.*, **14**, N36-N40.

Distribution

**No. of
Copies**

**No. of
Copies**

OFFSITE

Mr. W. Randy Bell
United States DOE
NNSA/NA-22
1000 Independence Ave. SW
Washington, DC 20585

Dr. David Berry
United States DOE
NNSA/NA-22
1000 Independence Ave. SW
Washington, DC 20585

LTC Ariel Cuadrado
United States DOE
NNSA/NA-22
1000 Independence Ave. SW
Washington, DC 20585

Dr. Victoria T. Franques
United States DOE
NNSA/NA-22
1000 Independence Ave. SW
Washington, DC 20585

Mr. Ralph Hastings
United States DOE
NNSA/NA-22
1000 Independence Ave. SW
Washington, DC 20585

Mr. Eric Sanders
United States DOE
NNSA/NA-22
1000 Independence Ave. SW
Washington, DC 20585

Dr. Vaughn Standley
United States DOE
NNSA/NA-22
1000 Independence Ave. SW
Washington, DC 20585

Dr. Rhys M. Williams
United States DOE
NNSA/NA-22
1000 Independence Ave. SW
Washington, DC 20585

ONSITE

13 Pacific Northwest National Laboratory

Anheier, NC (4)	K5-25
Bernacki, BE	K5-25
Bruckner-Lea, C	K5-25
Clemmer, RG	K8-02
Dudder, GB	K8-29
Krishnaswami, K	K5-25
Schultz, JF	K5-25
Sharpe, SW	K8-88
Information Release Office (2)	K1-06